Chemical Engineering Research and Design 207 (2024) 100–109

Contents lists available at ScienceDirect

Chemical Engineering Research and Design

journal homepage: www.elsevier.com/locate/cherd

Performance optimization of adsorption hydrogen storage system via computation fluid dynamics and machine learning

Chuchuan Peng, Xianyang Liu, Rui long *, Zhichun Liu, Wei Liu

School of Energy and Power Engineering, Huazhong University of Science and Technology, Wuhan 430074, China

ARTICLE INFO

Keywords:
Adsorption hydrogen storage
Fin configuration
Heat and mass transfer
Machine learning

ABSTRACT

Adsorption hydrogen storage paves an alternative way for reliable hydrogen storage. Here, impacts of dimensionless fin geometry configurations of the fin-tube metal hydride bed on the hydrogen storage performance are systematically investigated. Results show employing fins can strengthen the heat and mass transfer characteristics in the adsorbent bed and shorten the adsorption duration, especially at large fin numbers. Larger dimensionless fin thickness, height and width can lower the average bed temperature, which contributes to the adsorption kinetics and hydrogen fraction. At a small adsorption duration, larger dimensionless fin thickness, height and width improve the hydrogen storage amount due to obviously augmented hydrogen fraction. At a larger adsorption duration, there exist optimal dimensionless fin thickness, height and width leading to the maximum hydrogen storage amount originating from the compromise between the hydrogen fraction and adsorbent filled. Based on machine learning, the relationships between dimensionless fin geometry parameters and hydrogen storage amount have been obtained, and the optimal adsorption duration depended dimensionless fin configurations are obtained based on genetic algorithm. At a moderate adsorption duration, the optimized finned bed can significantly enhance the hydrogen storage amount. At the adsorption duration of 400 s, the hydrogen storage amount is augmented by 12.8%.

1. Introduction

Hydrogen is regarded as a promising candidate for energy revolution and transformation, which can significantly contribute to achieving the carbon neutrality commitment. Efficient and safe hydrogen storage is highly demanded for hydrogen utilization. There are mainly three mature hydrogen storage technologies: high-pressure gaseous hydrogen storage, cryogenic liquid hydrogen storage and solid adsorption hydrogen storage (Baetcke and Kaltschmitt, 2018; Kazeem et al., 2020). Compared with other hydrogen storage technologies, adsorption hydrogen storage presents advantages of good safety (Sakintuna et al., 2007; Wang et al., 2022a), large volumetric density (~1.5–11 wt%) (Jana and Muthukumar, 2021) and convenient transportation, where metal hydrides (MHs) are usually employed as the adsorbents (Luo et al., 1998; Wjihi et al., 2017).

The adsorption hydrogen storage performance is affected by the heat and mass transfer characteristics in the adsorbent bed (Shen and Zhao, 2013; Yang et al., 2008). Factors impacting the heat and mass transfer characteristics mainly lies in hydrogen injection speed (Mohammadshahi et al., 2016a), hydrogen supply pressure (Jiao et al., 2012; Kumar et al., 2021; Mohan et al., 2007) and external cooling fluid temperature (Bao et al., 2013; Patil and Ram Gopal, 2013; Souahlia et al., 2014), the shape and material of the reaction chamber (Wang and Brinkerhoff, 2021), the particle radius and porosity of hydrogen storage materials (Li et al., 2020; Lin et al., 2019). The details of the various MH reactors in previous researches are listed in Table 1.

Regarding to the safety issues and experiment costs, mathematical models have been widely employed to describe the hydrogen adsorption process (Hardy and Anton, 2009; Muthukumar et al., 2009). Nakagawa et al. demonstrated that the assumption of the local gas temperature equal to the bed temperature is validated in a two-dimensional transient model (Nakagawa et al., 2000). Na Ranong et al. applied Danckwerts-type boundary conditions to the modeling of MH reactors (Na Ranong et al., 2011). Song et al. proposed a new kinetics model called the varying-size model, which accurately describes the kinetics process of the gas–solid reaction, particularly for processes with apparent volumetric deformation (Song et al., 2018). Chung et al. investigated the influence of expansion volume and thermal convection

* Corresponding author.
E-mail address: r_long@hust.edu.cn (R. long).

https://doi.org/10.1016/j.cherd.2024.05.022
Received 14 July 2023; Received in revised form 3 March 2024; Accepted 15 May 2024
Available online 19 May 2024

on the adsorption process (Chung and Ho, 2009). Demircan et al. developed a two-dimensional mathematical model with complex heat and mass transfer and fluid flow considered (Demircan et al., 2005). Considering the neglected key physical influences in previous studies, Nam et al. developed a 3D MH model (Nam et al., 2012). Mohammadshahi et al. improved the traditional mathematical model of the MH tank system, which can predict experimental configurations more accurately (Mohammadshahi et al., 2016b).

Much efforts have also been devoted to ameliorating the hydrogen storage performance regarding to the adsorbent bed (Dhaou et al., 2010; Garrison et al., 2012; Keshari and Maiya, 2018; Manai et al., 2019; Raju and Kumar, 2012). There are two commonly improved methods. One is changing the parameters and shape of fin in MH tank. The other is increasing the convective heat transfer area between cooling fluid and tank. Both of them can reduce the thermal resistance and remove the reaction heat quickly from tank, which benefits to the positive progress of the reaction. This allows for fast hydrogen storage. Mellouli et al. studied the influence of fin spacing, length, thickness and arrangement on the hydrogen filling process of vehicle MH storage tanks equipped with finned spiral tube heat exchangers. With other parameters constant, the rate at which hydrogen is absorbed in 13 mm fin length is rapid compared to the other values (5 and 10 mm). The hydride powder at which hydrogen is absorbed in 4 mm fin thickness has faster heat transfer rate compared to 2 and 3 mm. At fin pitch of 5 mm, the hydride temperature approaches the cooling fluid temperature quickly than 10 and 15 mm (Mellouli et al., 2010). A good choice of these parameters can contribute to heat transfer, which consequently facilitates hydrogen absorption. Nyamsi et al. found that the thermal resistance of the whole heat exchanger can be diminished by increasing the fin radius and decreasing the fin thickness. They further analyzed the impact of cooling tube diameter and fin length on hydrogen charging time. The hydrogen charging time is reduced by 25% when the tube diameter increases from 2.5 mm to 5 mm. The increasing of cooling tube increases the heat transfer surface area between the tube and the hydride powder. Besides, the heat transfer rate from a single fin is proportional to the tube diameter according to their calculations. Therefore, the increasing of cooling tube diameter results in a reduction of hydrogen charging time. With the augment of fin length, the thermal resistance and hydrogen charging time are reduced by 13% and 42%, respectively (Nyamsi et al., 2012). Chandra et al. concluded that tapered fins provide better heat transfer than circular fins with the same outer and inner diameters owing to their extra surface area. The time required for cooling and saturation is reduced at larger number of fins or tubes (Chandra et al., 2020). Ma et al. found that the thermal resistance of reaction system decreases with increasing fin radius, thickness and number (Ma et al., 2014). Wang et al. optimized the conical fins to improve the heat transfer performance. The optimized conical fin has more heat transfer quantity and higher fin efficiency compared with those of some typical fins (Wang and Wang, 2016). Wang et al. developed a MH device with novel corrugated fins. The wavy fin configuration presents better hydrogen adsorption performance than the traditional circular fin configuration due to larger thermal contact surface (Wang et al., 2022b). Bai et al. introduced tree fins to ameliorate the heat transfer characteristics. Compared with radial fins, the hydrogen adsorption time is almost reduced by 20.7% under the condition of 90% saturation due to better heat transfer performance (Bai et al., 2021). Krishna et al. focused on novel bio-inspired leaf-vein type fins for the MH reactor. They found that the inclined fin configuration presents better performance (Krishna et al., 2022). An increase in angle reduces the heat conduction distance between the fins near the periphery and improves the heat transfer performance. Singh et al. revealed that increasing the number and thickness of fins augments the hydrogen adsorption rate and diminishes hydrogen charging time due to the small heat conduction path between the fins (Singh et al., 2015).

It has been demonstrated that introducing fins into the adsorbent bed can improve the heat and mass transfer characteristics in the adsorbent bed in the adsorption-based energy transformation systems. Here the hydrogen storage performance in the fin-tube adsorption bed is investigated. The impacts of dimensionless fin geometry configurations (such as dimensionless fin number, height, width, and length) on the bed temperature, hydrogen fraction, and hydrogen storage amount are systematically discussed. Machine learning is employed to construct the underling adsorption duration depended relationships between the fin geometry parameters and the hydrogen storage amount. The optimal adsorption duration depended fin configurations are further identified through genetic algorithm. This study contributes to rational design and

Table 1
Summary of hydrogen storage performance of different MH reactors reported in the literature.

Reference	Reactor	Material	Operating conditions	Hydrogen storage performance
(Mohammadshahi et al., 2016a).	Cylindrical reactor with copper fins and cooling tube	$LaNi_5$	The cooling fluid temperature $T_c = 303$ K, the supply pressure $P_s = 0.1$ bar	It takes 5 h to reach 1.5 wt% hydrogen storage when the 1.65 kg hydrogen is injected in 5 h.
(Jiao et al., 2012).	Cylindrical reactor	$LaNi_5$	$T_c = 293$ K, the initial temperature $T_0 = 293$ K, $P_s = 2$–20 bar, the convective heat transfer coefficient $h = 300$ W/m^2·K	The overall absorbed hydrogen fraction can reach up to 0.38 within 120 s.
(Kumar et al., 2021).	Cylindrical reactor with embedded cooling tubes	$MmNi_{4.7}Fe_{0.3}$	$P_s = 10$–70 bar, $T_c = 298$ K	The storage reactor can stock 45.984 g hydrogen in 676 s, at 70 bar supply pressure.
(Mohan et al., 2007).	Cylindrical reactor with embedded cooling tubes	$LaNi_5$	$P_s = 8$–15 bar, $T_c = 293$–323 K, $h = 500$–1500 W/m^2·K	The configuration with 55 cooling tubes attains a storage capacity of approximately 1.2 wt% in 5000 s, subjected to 15 bar supply pressure and 300 K cooling fluid temperature.
(Bao et al., 2013).	2D axisymmetric reactor with a central heat exchanger tube	Mg	$T_c = 473$–593 K, $P_s = 1.2$ MPa	The reactor approaches saturation within 1100 s at 473 K.
(Patil and Ram Gopal, 2013).	Cylindrical reactor	$MmNi_{4.6}Al_{0.4}$	$T_c = 298$ K, $P_s = 30$ bar, $h = 1000$ W/m^2·K	The reactor is able to store 90% of the maximum storage capacity in 247 s when the bed concentration at the beginning of adsorption is 10%.
(Souahlia et al., 2014).	Annular cylindrical vessel with finned spiral coil	$LaNi_5$	$P_s = 3$–11 bar, $T_c = 273$–353 K	The MH tank is able to attain a storage capacity of approximately 1.34 wt% in nearly 433 s, under an adsorption condition of 11 bar, 293 K
(Wang and Brinkerhoff, 2021).	Cylindrical reactor	$LaNi_5$	$T_0 = 293$ K, the initial pressure $P_0 = 10$ bar	A 5–25% decrease in adsorption time is noted when the aspect ratio of the reactor chamber is 5.
(Li et al., 2020).	Fixed bed tubular reactor with thermostatic bath	$LaNi_5$	$T_c = 363$–423 K, $P_s = 0.1$ MPa	The largest dehydriding capacity of $LaNi_5$ reaches 0.95 wt% within 10 s at 423 K compared with other working temperatures.
(Lin et al., 2019).	Cylindrical reactor with water bath cooling	$LaNi_5$	$T_c = T_0 = 293$ K, $P_s = 1$ MPa, $h = 1652$ W/m^2·K	90% of hydrogen can be adsorbed within 499.23 s when the particle radius is 100 μm and the porosity is 0.6.

fabrication of fin-tube adsorption bed for efficient hydrogen storage.

2. Model and methods

As shown in Fig. 1, a coaxial cylindrical reactor is considered here (Muthukumar et al., 2007). The inner tube of the cylindrical reactor is a porous filter tube that acts as a hydrogen channel and distributor, preventing the hydride particles from being carried away by hydrogen flow. $LaNi_5$ is filled in the annular space between the filter tube and the concentric tube. The cooling fluid flows in the space near the outer wall. Fins are installed attached to the outer wall of the MH bed. The material of fins is steel. Fig. 1(b) shows the geometric parameters of fins. The dimensionless fin thickness θ/θ_1, height R/R_1 and width L/L_1, are employed to describe the fin geometric controlling parameters. R_1 is 16 mm. L_1 is 20 mm. θ_1 is determined by the fin number.

2.1. Mathematical model

The assumptions of the employed mathematical model in this study are as follows (Chandra et al., 2020):

(1) The gas phase is treated as ideal gas.
(2) There is no heat transfer through the porous filter
(3) The thermal properties of hydride bed are independent of bed temperature and hydrogen supply pressure. Specific heat and thermal conductivity of materials are invariable in this paper.

2.1.1. Reaction kinetic equation

The adsorption reaction of adsorption hydrogen storage is described as

$$LaNi_5 + 3H_2 \leftrightarrow LaNi_5H_6 + \text{heat}$$

The reaction rate depends on bed temperature, hydrogen pressure and hydrogen fraction in the hydride bed. The reaction kinetics is given by (Chandra et al., 2020; Yang and Zhang, 2011)

$$\frac{\partial W}{\partial t} = C_a \exp\left(\frac{-E_a}{R_u T}\right) \ln\left(\frac{p}{p_{eq}}\right)(1 - W) \tag{1}$$

where W is the hydrogen fraction. The equilibrium pressure p_{eq}can be calculated as (Chandra et al., 2020; Yang and Zhang, 2011; Anbarasu et al., 2014; Muthukumar et al., 2012)

$$p_{eq} = \exp\left[\frac{\Delta S}{R_u} - \frac{\Delta H}{R_u T} + (\varphi + \varphi_o) \times \tan(\pi(W - 0.5)) + \frac{\beta}{2}\right] 10^5 \mathrm{N/m^2} \tag{2}$$

2.1.2. Mass conservation equation

The mass conservation equation for hydrogen is given by (Chandra et al., 2020; Anbarasu et al., 2014; Muthukumar et al., 2012; Busque et al., 2017, 2018)

$$\varepsilon \frac{\partial \rho_g}{\partial t} + \nabla(\rho_g \cdot \vec{u}) = -S_{mass} \tag{3}$$

where ρ_g is the gas density, which can be derived via the ideal gas model

$$\rho_g = \frac{pM_g}{R_u T} \tag{4}$$

The mass conservation equation for MH is (Chandra et al., 2020; Busque et al., 2017, 2018)

$$(1 - \varepsilon)\frac{\partial \rho_{MH}}{\partial t} = S_{mass} \tag{5}$$

The mass source term can be calculated as (Chandra et al., 2020; Anbarasu et al., 2014; Muthukumar et al., 2012; Busque et al., 2017, 2018)

$$S_{mass} = C_a \exp\left(\frac{-E_a}{R_u T}\right) \ln\left(\frac{p}{p_{eq}}\right)(\rho'_{sat} - \rho'_{MH}) \tag{6}$$

where ρ'_{sat} and ρ'_{MH} are the effective densities of MH bed at saturation state and at any time respectively

$$\rho'_{sat} = \rho_{sat}(1 - \varepsilon) \tag{7}$$

$$\rho'_{MH} = \rho_{MH}(1 - \varepsilon) \tag{8}$$

where the saturated MH density is calculated as $\rho_{sat} = \rho_i \cdot (1 + wt\%_{sat})$.

2.1.3. The momentum equation

A bulk approximation of the Brinkman equation is given by (Lesmana and Aziz, 2023)

$$\frac{\rho_g}{\varepsilon}\frac{\partial \vec{u}}{\partial t} + \frac{\rho_g}{\varepsilon}\vec{u}\nabla\vec{u} = -\nabla p + \nabla\left[\frac{\mu}{\varepsilon}\left(\nabla\vec{u} + (\nabla\vec{u})^T\right) - \frac{2\mu}{3\varepsilon}\nabla\vec{u}I\right] - \frac{\mu}{K}\vec{u} - \beta_f|\vec{u}|\vec{u} - \frac{S_m}{\varepsilon^2} + \rho_g\vec{g} \tag{9}$$

Here, the gravity force term is not taken into consideration. The equation can be simplified by using several assumptions mentioned previously. Due to very low hydrogen velocity (Reynolds number < 1), the inertial term can be neglected as it is almost undetectable compared to viscous force. The Kn<0.1 in our simulation conditions. Therefore the Knudsen diffusivity is neglected. We can also neglect and remove the

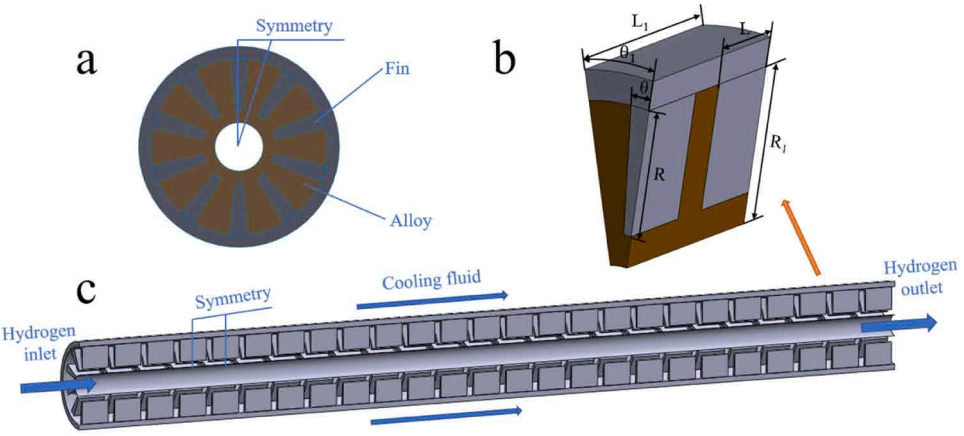

Fig. 1. Structure of coaxial cylindrical reactor.

Forchheimer drag effect (β_f) from the equation. With above considerations, the expression can be simplified as

$$\frac{\rho_g}{\varepsilon}\frac{\partial \vec{u}}{\partial t} = -\nabla p + \nabla\left[\frac{\mu}{\varepsilon}\left(\nabla\vec{u} + (\nabla\vec{u})^T\right) - \frac{2\mu}{3\varepsilon}\nabla\vec{u}l\right] - \frac{\mu}{K}\vec{u} - \frac{S_m}{\varepsilon^2} \tag{10}$$

where μ is the dynamic viscosity of gas. K is bed permeability

$$K = \frac{d_p^2\varepsilon^3}{150(1-\varepsilon)^2} \tag{11}$$

where d_p is the particle size of the MH.

2.1.4. Energy conservation equation

The energy conservation equation in the MH bed is (Chandra et al., 2020; Anbarasu et al., 2014; Muthukumar et al., 2012; Busque et al., 2017, 2018)

$$\rho c_p\frac{\partial T}{\partial t} + (\rho c_p)_g(\vec{u}\cdot\vec{\nabla}T) = k\nabla^2 T + S_{heat} \tag{12}$$

where

$$\rho c_p = \varepsilon(\rho c_p)_g + (1-\varepsilon)(\rho c_p)_{MH} \tag{13}$$

$$k_{eff} = \varepsilon k_g + (1-\varepsilon)k_{MH} \tag{14}$$

The heat source term is calculated by (Chandra et al., 2020; Anbarasu et al., 2014; Muthukumar et al., 2012)

$$S_{heat} = S_{mass}\frac{\Delta H}{M_g} \tag{15}$$

Table 2
Relevant parameters in the model.

Name	Symbol	Value	Reference
Activation energy for adsorption	E_a	21179.6 J/mol	(Chandra et al., 2020; Singh et al., 2017)
Reaction rate constant	C_a	59.187 s^{-1}	(Mohammadshahi et al., 2016b; Chandra et al., 2020)
Slope factor	φ	0.038	(Chandra et al., 2020; Singh et al., 2017)
	φ_o	0	(Chandra et al., 2020)
Hysteresis factor	β	0.137	(Chandra et al., 2020; Singh et al., 2017)
Initial density of alloy	ρ_i	8400 kg/m^3	(Mohammadshahi et al., 2016b)
Weight fraction of maximum absorbed hydrogen	$wt\%_{sat}$	1.4%	(Chandra et al., 2020)
Specific heat of metal hydride	C_{pMH}	419 J/(kg K)	(Singh et al., 2017)
Thermal conductivity of metal hydride	k_{MH}	2.4 W/(m K)	(Singh et al., 2017; Boukhari and Bessaïh, 2015)
Hydrogen gas specific heat	C_{pg}	14283 J/(kg K)	(Muthukumar et al., 2007)
Thermal conductivity of hydrogen	k_g	0.18 W/(m K)	(Singh et al., 2017)
Molar mass of hydrogen	M_g	0.002 kg/mol	(Chandra et al., 2020)
Enthalpy of formation	ΔH	30800 J/mol	(Chandra et al., 2020)
Mean particle size	d_p	1.825×10^{-5} m	(Nyamsi et al., 2012)
Entropy of formation	ΔS	108 J/(mol K)	(Chandra et al., 2020)
Porosity	ε	0.5	(Muthukumar et al., 2007; Singh et al., 2017)
Fin thermal conductivity	k_f	15 W/(m K)	(Singh et al., 2017)
Fin material density	ρ_f	7900 kg/m^3	(Singh et al., 2017)
Fin specific heat	C_{pf}	460 J/(kg K)	(Singh et al., 2017)

2.2. Initial conditions and boundary conditions

Relevant parameters involved in the model are shown in Table 2. The tank and fin material are steel. The initial temperature and pressure of the MH bed are 293.15 K and 10 bar, respectively. Based on the symmetry of the reactor, the computation domain is shown in Fig. 1(b). The front, back, left and right surfaces are set as symmetrical boundaries. The inner wall is set as the pressure inlet boundary at a pressure of 10 bar. The adsorption heat is transferred to the outer wall. The coolant is set at 293 K, and the convective heat transfer coefficient is 1000 W/m^2·K (Muthukumar et al., 2007, 2012). The mesh independence and model validation can be found in the Supplementary Material file.

2.3. Mesh independence and model validation

The above governing equations are solved via COMSOL Multiphysics with appropriate boundary conditions. The calculation domain is meshed with hexahedral elements. Mesh independence verification is carried out by calculating the main performance indicators such as average bed temperature and hydrogen fraction under various numbers of mesh numbers. In the calculation, the dimensionless fin thickness, height and width are set as 0.1, 1 and 0.05, respectively. The average bed temperature and hydrogen fraction under different mesh numbers are shown in Fig. S1 in the Supplementary Material file. It can be seen that the average temperature and hydrogen fraction under different mesh numbers are nearly coincident. The difference of hydrogen fraction under different mesh numbers and adsorption durations is less than 0.001; And the difference of the average bed temperature is less than 0.1 K. Therefore, a mesh number of 36,162 is employed in the following calculations, which is sufficient to guarantee accurate results.

In order to validate the accuracy of the numerical model employed, under the same geometry model in Ref (Cao et al., 2013)., the numerical results are compared with the experimental ones. As shown in Fig. S2 in the Supplementary Material file, the calculated hydrogen fractions under agree well with the experimental ones, which validates the employed numerical model.

3. Impacts of fin geometric configuration on the hydrogen storage performance

3.1. Impacts of fin numbers

Here, the dimensionless fin thickness θ/β, height R/R_1 and width L/L_1 are set as 0.3, 0.8 and 0.4, respectively. Under different fin numbers, the time-depended average bed temperature, hydrogen fraction and hydrogen storage amount are shown in Fig. 2. At the beginning of the adsorption process, the adsorption is rather strong, releasing a large amount of adsorption heat. The average temperature of the bed rises to 340 K rapidly until 50 s. The average temperature will keep above 340 K if there is no coolant and fin as shown in Fig. S3. The adsorption heat can be transferred to the outside wall and carried away by the cooling fluid. The heat dissipation rate is greater than the adsorption heat generation rate. The average bed temperature gradually decreases. From 50 s to 1000 s, the average temperature decreases to 295 K rapidly for finned beds. When the adsorption heat generation rate and heat dissipation rate tend to be in equilibrium, the average temperature stays nearly unchanged (~294 K). At the same adsorption duration, the average bed temperature decreases gradually with the increasing fin numbers. Employing fins augments the high heat conduction area of the adsorbent bed. The adsorption heat can be more easily transferred to the outside wall and carried away by the cooling water. The average temperature of 5-finned bed and 10-finned bed is 14.4 K and 17.1 K lower than that of bed without fins at the adsorption duration of 800 s, respectively.

As shown in Fig. 2(b), the hydrogen fraction increases gradually as the adsorption process progresses. The hydrogen fraction increases rapidly before 200 s. The increase rate is under 0.001/s after 800 s. At

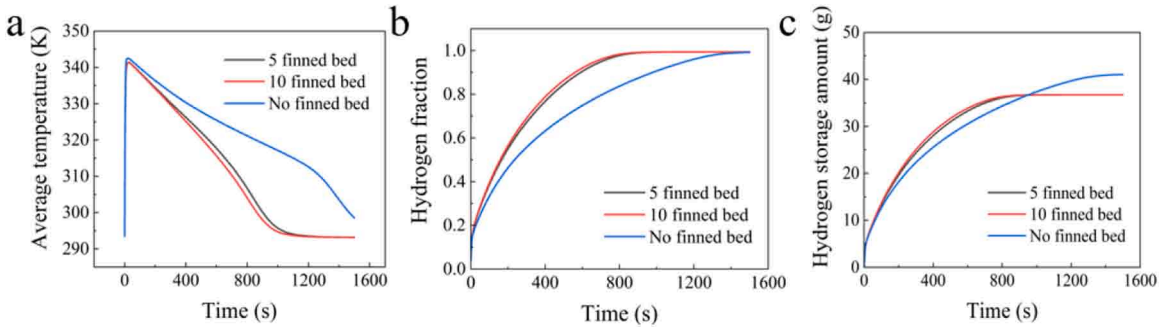

Fig. 2. The average temperature, hydrogen fraction, and hydrogen storage amount under different adsorption durations and fin numbers.

the same adsorption duration, the hydrogen fraction of the 10-finned bed is the largest, followed by the 5-finned bed, and the hydrogen fraction of the original non-finned bed is the smallest. Compared with the non-finned bed, employing fins lowers the bed temperature. Lower temperature is conducive to the reaction, leading to larger hydrogen fraction. The adsorbent reaches the saturation state more quickly. The adsorbent in 5-finned and 10-fined beds is saturated about 520 s and 560 s earlier than that in the non-finned bed, respectively. The required time for adsorbent saturation in the bed with fins is reduced by at least 36.4% compared to original bed without fins. Fig. 3 exhibits the temperature and hydrogen fraction contours at the adsorption duration of 500 s. The temperature near the inlet is above 340 K, whereas it is below 325 K near the fin and heat exchange wall. Meanwhile, the hydrogen fraction is opposite to the temperature distribution. More fins contribute to decreasing the bed temperature and augmenting the hydrogen fraction.

As depicted in Fig. 2(c), as the adsorption process proceeds, the hydrogen storage amount gradually increases. The hydrogen storage amount increases rapidly before 200 s. The increase amplitude of hydrogen storage decreases with time. Finally, the hydrogen storage amount remains stable at 36.7 g, which is consistent with the trend described in Fig. 2(b). The hydrogen storage amount in 5-finned bed and the 10-finned bed is much larger than that in the non-finned bed from 300 s to 800 s. The hydrogen storage amount of 5-finned bed and 10-finned bed is 5% and 5.7% more than that of bed without fins at the adsorption duration of 800 s, respectively. Employing fins diminishes the effective volume for the filled adsorbent, leading to reduced saturated hydrogen storage amount.

3.2. *Impacts of dimensionless fin thickness*

Here, the dimensionless fin height and width are fixed at 0.8 and 0.4, respectively. Due to the definition of the dimensionless fin thickness, the same dimensionless fin thickness leads to the equal amount of adsorbent filled in the adsorbent bed. Fig. 4 shows the relations of average bed temperature and the dimensionless fin thickness at different adsorption durations. The average temperature of the 10-finned bed is lower than that of the 5-finned bed. At the given dimensionless fin height and width, the proportion of high heat conductive zone increases with the increase of dimensionless fin thickness. At 500 s and 800 s, the average

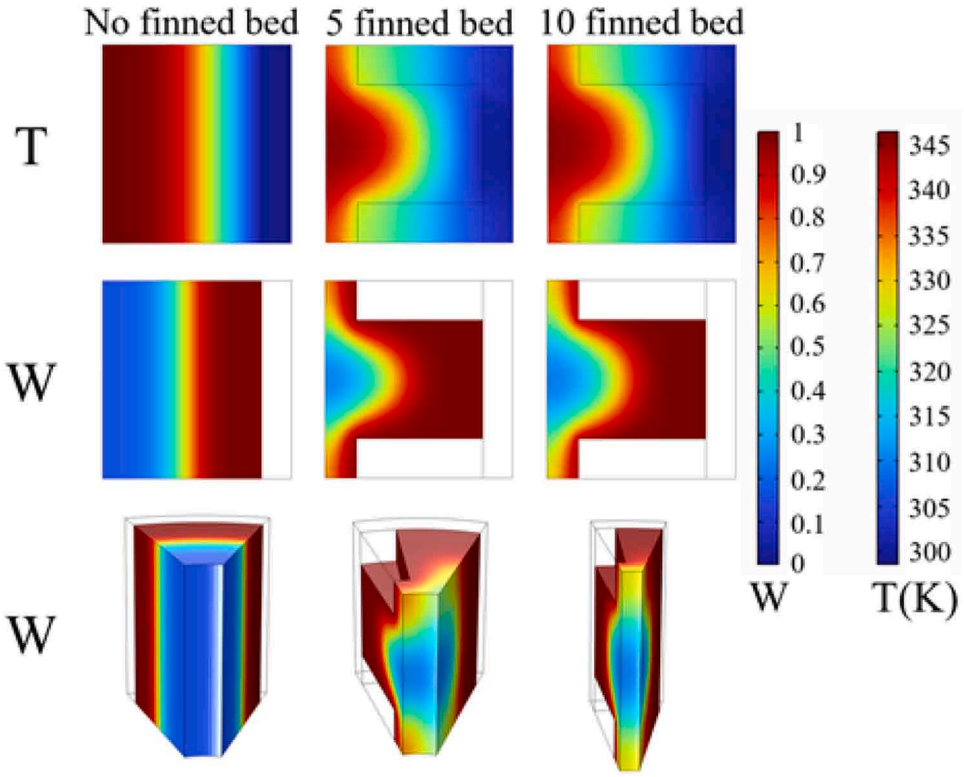

Fig. 3. Temperature and hydrogen fraction contours under different fin numbers at the adsorption duration of 500 s.

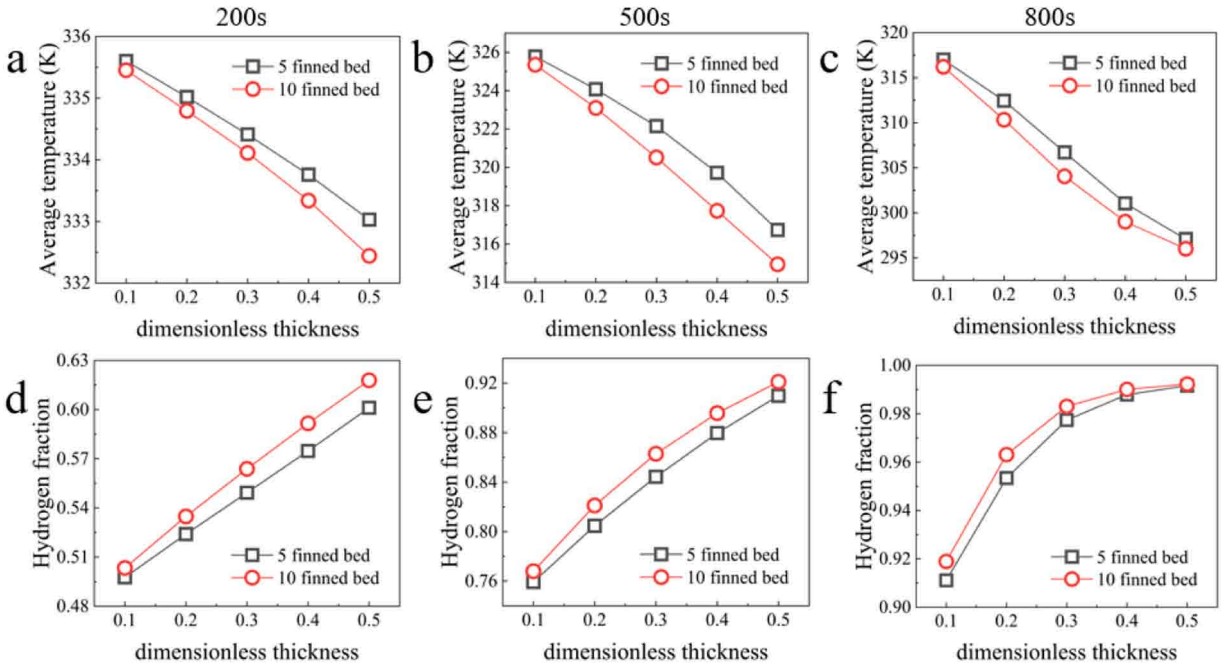

Fig. 4. The relationship of average temperature and hydrogen fraction with dimensionless fin thickness.

temperature difference between 5-finned and 10-finned beds is rather small at a dimensionless fin thickness of 0.1. With the increase of dimensionless fin thickness, obvious difference of average temperature between 5-finned and 10-finned bed can be observed. Fig. 4(d-f) show the variation of hydrogen fraction with dimensionless fin thickness under different adsorption durations. At the same adsorption duration, the hydrogen fraction of the MH bed increases with the increase of dimensionless fin thickness. As the dimensionless fin thickness increases, high heat conduction zone extends. The generated adsorption heat can be more easily transferred to the outside wall and taken away by the cooling fluid. Therefore, the bed temperature decreases. It contributes to the adsorption driving force, which leads to larger hydrogen fraction. Under the same dimensionless fin thickness, the hydrogen fraction of 10-finned bed is larger than that of 5-finned bed. The difference is below 0.01 at 800 s. The hydrogen fraction distributions for different dimensionless fin thickness at the adsorption duration of 500 s are shown in Fig. S5 in the Supplementary Material file. The areas of low hydrogen fraction are lessened with augmented dimensionless thickness. The average temperature for 10-finned bed at a dimensionless thickness of 0.5 is 20 K lower than that at a dimensionless thickness of 0.1 at 800 s; The hydrogen fraction for 10-finned bed at a dimensionless thickness of 0.5 is 0.07 more than that at a dimensionless thickness of 0.1.

As shown in Fig. 5, at the given dimensionless fin height and width, the hydrogen storage amount of bed varies with the dimensionless fin thickness at different adsorption durations. The hydrogen storage amount is determined by the hydrogen fraction and the amount of adsorbent filled. At a small dimensionless fin thickness (e.g. 0.1), the hydrogen fraction of the bed is very low, leading to a small hydrogen storage amount. At a larger dimensionless fin thickness (e.g. 0.4), although the hydrogen fraction of 10-finned bed is about 0.9 at 500 s, due to the increase of fin thickness, the filled adsorbent decreases more obviously, resulting in lowered hydrogen storage amount. Therefore, there exists an optimal value of thickness for hydrogen storage amount at the adsorption duration of 500 s and 800 s, respectively. At 200 s and 500 s, the hydrogen storage amount in the 10-finned bed is higher than that in the 5-finned bed due to better constructed effective thermal conductance network in the 10-finned configurations. Under a dimensionless thickness of 0.3, the hydrogen storage amount for 10-finned bed

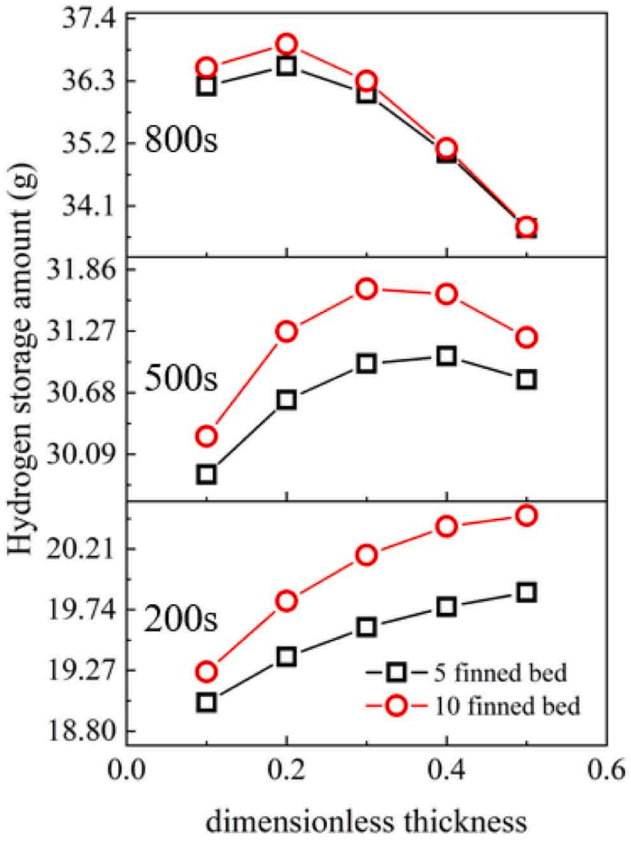

Fig. 5. The relationship between hydrogen storage amount and the dimensionless fin thickness.

is 2.3% more than that for 5-finned bed at the adsorption duration of 500 s. The hydrogen storage amount of the 10-finned bed coincides with that of the 5-finned bed as the adsorbent is near saturated at 800 s. The hydrogen storage amount for 10-finned bed at a dimensionless thickness of 0.2 is 9.6% more than that at a dimensionless thickness of 0.5 at the

adsorption duration of 800 s.

3.3. Impacts of dimensionless fin height

Here the dimensionless fin thickness and width are set as 0.3 and 0.4, respectively. The relationship of average temperature of beds with the dimensionless fin height under different adsorption durations are shown in Fig. S7 in the Supplementary Material file. The increase of dimensionless fin height extends the high thermal conductivity area, which is beneficial to remove the adsorption heat, resulting in lower average temperature. Due to better thermal conductance network under the 10-finned configuration, its average bed temperature is lower than that of the 5-finned bed. The hydrogen fractions of two beds increase with the increase of the dimensionless fin height. For the 10-finned bed, better thermal conductance network is constructed, leading to a large contact area between the adsorbent and the fins. The adsorption heat of absorbent near the inlet surface can be more efficiently conducted through fins. As shown in Fig. S8 in the Supplementary Material file, a region of small hydrogen fraction (under 0.65) is formed at a small dimensionless fin height. At a dimensionless fin height of 1, the hydrogen fractions are more than 0.8 at the adsorption duration of 800 s. The average temperature for 10-finned bed at a dimensionless height of 1 is 17 K lower than that at a dimensionless height of 0.2; the hydrogen fraction for 10-finned bed at a dimensionless height of 1 is 0.12 more than that at a dimensionless height of 0.2.

The variation of the hydrogen storage amount with the dimensionless fin height at different adsorption durations is shown in Fig. 6. The hydrogen storage amount increases with the increase of dimensionless fin height. The increase of hydrogen fraction has a more significant impact on hydrogen storage amount compared to the decrease of absorbent at 200 s and 500 s. Therefore, the hydrogen storage amount

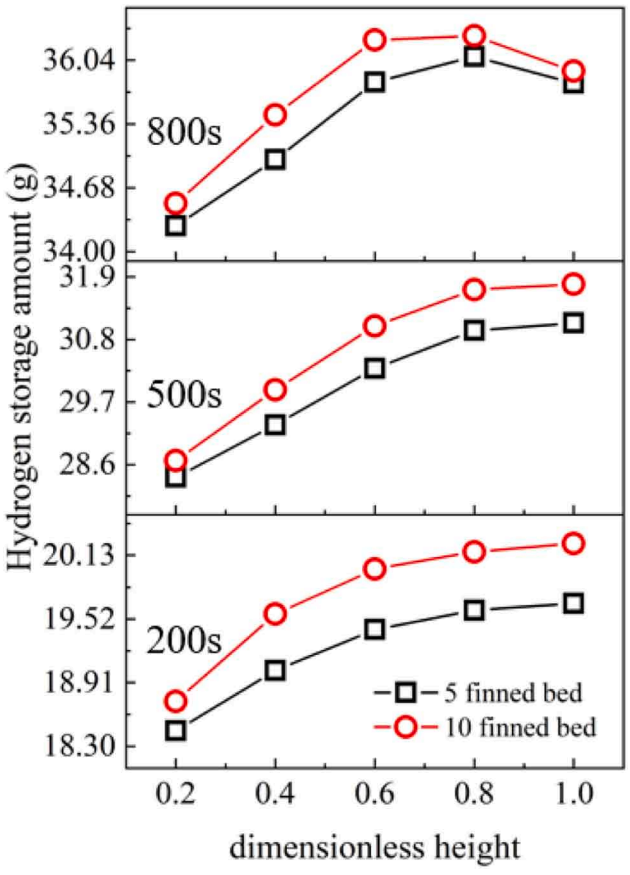

Fig. 6. The relationship between hydrogen storage amount and the dimensionless fin height.

augments with increasing dimensionless fin height. Although the hydrogen fraction increases with the increase of dimensionless height at 800 s, the adsorbent filled in the bed decreases more significantly, which reduces the hydrogen storage amount. The hydrogen storage amount for 10-finned bed at a dimensionless height of 0.8 is 5.2% more than that at a dimensionless height of 0.2 at the adsorption duration of 800 s. The hydrogen storage amount of the 10-finned bed is higher than that of the 5-finned adsorption bed due to better heat and mass transfer performance. The hydrogen storage amount for 10-finned bed at a dimensionless height of 1 is 2% more than that for 5-finned bed at the adsorption duration of 500 s. The difference of the storage amount of the two finned beds is not obvious as the adsorbent is close to the saturation state after 800 s. For Eq. (1), p and W of the beds get close to p_{eq} and 1 as adsorption approaches the equilibrium, respectively. Therefore, the adsorption driving force reduces. The adsorption rate decreases to 0.01 g/s at 800 s, which approaches 0 later.

3.4. Impacts of dimensionless fin width

As shown in Fig. S9 in the Supplementary Material file, it can be seen that the average bed temperature decreases with increasing dimensionless fin width. Larger dimensionless fin width augments the volume of the high thermal conductivity area. The adsorption heat can be easily transferred to the outer wall, which lowers the bed temperature. The average bed temperature of the 10-finned bed is lower than that of the 5-finned bed due to more efficient heat conductance network constructed. The hydrogen fraction increases with the increase of the dimensionless fin width, as lower temperature is more favorable to the adsorption. As depicted in Fig. S10 in the Supplementary Material file, the adsorption heat of absorbent near the inlet surface can be more efficiently conducted through fins with increasing dimensionless fin width. Therefore, a region of small hydrogen fraction (less than 0.6) is formed at a small dimensionless fin width under 0.3. When the dimensionless fin width is 0.4, the hydrogen fractions of two bed are both larger than 0.7 at the adsorption duration of 800 s. The average temperature for 10-finned bed at a dimensionless width of 0.4 is 15 K lower than that at a dimensionless width of 0.05; The hydrogen fraction for 10-finned bed at a dimensionless width of 0.4 is 0.11 more than that at a dimensionless width of 0.05. The difference of average temperature and hydrogen fraction for two beds increases with the increase of the dimensionless fin width.

At different adsorption durations, the variation of hydrogen storage amount with the dimensionless fin width is shown in Fig. 7. The hydrogen fraction increases with increasing dimensionless fin width at the adsorption duration of 200 s and 500 s. Although the adsorbent filled decreases with the increase of dimensionless fin width, the hydrogen storage amount of bed increases. The hydrogen storage amount for 10-finned bed at a dimensionless width of 0.4 is 2.3% more than that for 5-finned bed at the adsorption duration of 500 s. The adsorption is weak at the adsorption duration of 800 s, and the increase of hydrogen fraction does not change obviously with the dimensionless fin width. However, larger dimensionless fin width greatly reduces the adsorbent filled in the bed, which results in decreasing hydrogen storage amount. Therefore, at 800 s, the hydrogen storage amount increases first with increasing dimensionless fin width, reaches its maximum value, and then decreases. The hydrogen storage amount for 10-finned bed at a dimensionless width of 0.3 is 3.8% more than that at a dimensionless width of 0.05 at the adsorption duration of 800 s. The hydrogen storage amount of the 10-finned bed is higher than that of the 5-finned bed.

3.5. Machine learning

As discussed above, the hydrogen storage performance is significantly impacted by the adsorption duration and the fin geometries. In order to reveal the relationships between fin geometry parameters and adsorption hydrogen storage performance at each adsorption duration, machine learning is employed to construct the adsorption duration

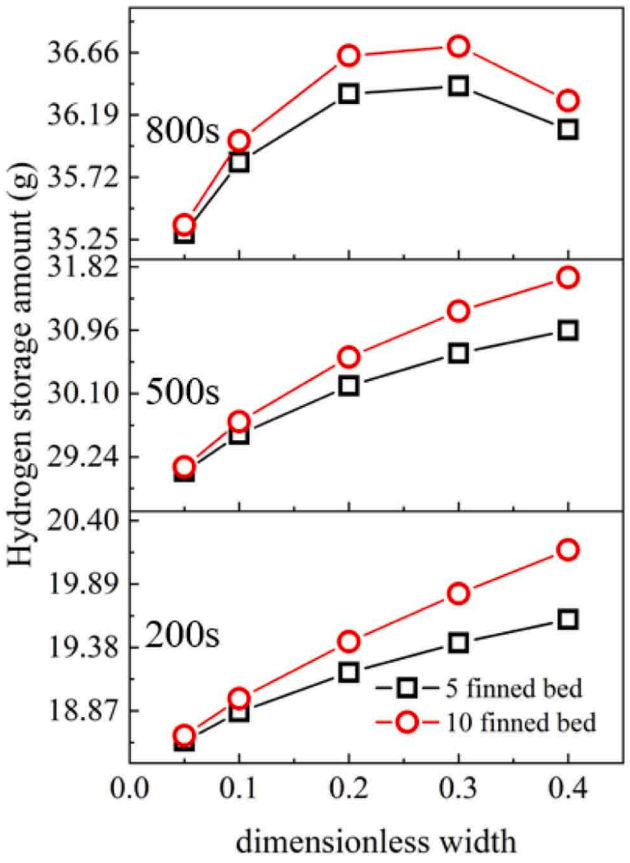

Fig. 7. The relationship between hydrogen storage amount and the dimensionless fin width.

depended relationships between fin height, width, thickness and hydrogen storage amount. The Principal Component Analysis (PCA) of parameters is depicted as Table 3. The process of machine learning is shown as Fig. S11. The ensemble-based regression model and decision tree regression model are applied. In the machine learning process, the hyperparameters of the model are optimized by Bayesian method. The training process is conducted several times to eliminate the random value. The actual and predicted values are shown in Fig. S12 in the Supplementary Material file. Performance indicators of different learning models are shown in Table 4. It can be seen that machine learning can well predict the performance of adsorption hydrogen storage system.

Furthermore, based on the adsorption duration depended relationships between the dimensionless thickness, height and width of fins and the hydrogen storage amount constructed by machine learning, the genetic algorithm is used to obtain the optimal configuration of fins at each adsorption duration thus to achieve the largest hydrogen storage amount. The optimal dimensionless geometric parameters of fins at different adsorption durations are shown in Table 5. The maximum adsorption duration depended hydrogen storage amount is shown in Fig. 8. The optimal hydrogen storage amount increases gradually with the increasing adsorption duration. At the adsorption duration of 400 s, the optimized finned bed can significantly enhance the hydrogen storage amount. The hydrogen storage amount is increased by 12.8%. The dimensionless fin volume (ratio of the fin volume and adsorption bed volume) can be calculated by:

$$\widehat{V} = \frac{1}{7}\left(\frac{\theta L}{\theta_1 L_1}\right)\left[22\left(\frac{R}{R_1}\right) - 8\left(\frac{R}{R_1}\right)^2\right]$$

The fin volume under the optimal configuration increases first with increasing adsorption duration, reaches the maximum value, then decreases due to the compromise between the hydrogen fraction and adsorbent filled.

Table 3
The Principal Component Analysis of parameters.

Parameter	thickness	height	width
Variation	68.0%	17.6%	14.4%

Table 4
Performance indicators of different machine learning models.

Machine learning model	RMSE	R2	MSE	MAE
Ensembles	0.2323	1.00	0.0540	0.182
Decision tree	0.2028	1.00	0.0411	0.163

Table 5
Optimal fin configuration under different adsorption durations.

Time (s)	Dimensionless thickness	Dimensionless height	Dimensionless width	Dimensionless volume
100	0.34826	0.5851	0.43059	0.217
200	0.51921	0.65709	0.2915	0.238
300	0.4043	0.8572	0.39213	0.294
400	0.69558	0.9851	0.47386	0.655
500	0.53291	0.7261	0.46896	0.420
600	0.17515	0.76012	0.47357	0.143
700	0.17675	0.80035	0.44936	0.142
800	0.15277	0.73156	0.43201	0.111

4. Conclusion

In this paper, effects of dimensionless fin number, thickness, height and width on average temperature, hydrogen fraction and hydrogen storage amount at different adsorption durations are systematically investigated by computational fluid dynamics. Machine learning is employed to construct the underling adsorption duration depended relationships between dimensionless fin geometry parameters and the hydrogen storage amount. The optimal adsorption duration depended fin configurations are identified through genetic algorithm. The main conclusions are listed below:

(1) Employing fins can strengthen the heat and mass transfer characteristics in the adsorbent bed and shorten the adsorption duration, especially at large fin numbers. Comparing to the original bed without fins, the required time for adsorption saturation in the 10-fined bed is reduced at least by 36.4%.
(2) Larger dimensionless fin thickness, height and width can lower the average bed temperature, which contributes to the adsorption process and augments the hydrogen fraction. At the adsorption duration of 800 s, the average temperature for 10-finned bed at a dimensionless width of 0.4 is 15 K lower than that at a dimensionless width of 0.05; The hydrogen fraction for 10-finned bed at a dimensionless width of 0.4 is 0.11 more than that at a dimensionless width of 0.05.
(3) At a small adsorption duration, larger dimensionless fin thickness, height and width can significantly improve the hydrogen storage amount due to obviously improved hydrogen fraction. At a larger adsorption duration, there exist optimal dimensionless fin thickness, height and width leading to the maximum hydrogen storage amount due to the compromise between the hydrogen fraction and adsorbent filled.
(4) Based on machine learning, the adsorption duration depended relationships between dimensionless fin geometry parameters and hydrogen storage amount has been obtained, and the optimal adsorption duration depended dimensionless fin configurations

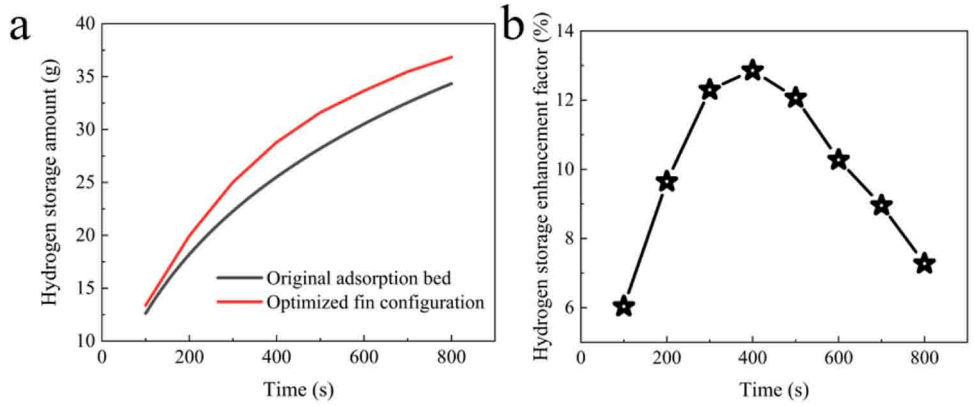

Fig. 8. The optimal adsorption duration depended adsorption hydrogen storage amount and hydrogen storage amount enhancement factor. The hydrogen storage enhancement is defined as the optimal hydrogen storage amount divided by that in the original configuration.

are obtained based on genetic algorithm. At a moderate adsorption duration, the optimized finned bed can significantly enhance the hydrogen storage amount. At the adsorption duration of 400 s, the hydrogen storage amount is augmented by 12.8%.

Declaration of Competing Interest

The authors declare that they have no known competing financial interests or personal relationships that could have appeared to influence the work reported in this paper.

Acknowledgements

This work was financially supported by the National Key Research and Development Program of China (2022YFB4003801).

Appendix A. Supporting information

Supplementary data associated with this article can be found in the online version at doi:10.1016/j.cherd.2024.05.022.

References

Baetcke, L., Kaltschmitt, M., 2018. Chapter 5 - Hydrogen Storage for Mobile Application: Technologies and Their Assessment. In: Azzaro-Pantel C, editor. Hydrog. Supply Chains: Acad. Press 167–206.
Kazeem S., Sobowale A., Oladapo O., Cyril O., Omoyemi A., Yommy A., et al. Hydrogen Storage Materials: A Review 2020.
Sakintuna, B., Lamari-Darkrim, F., Hirscher, M., 2007. Metal hydride materials for solid hydrogen storage: a review. Int. J. Hydrog. Energy 32 (9), 1121–1140.
Wang, F., Huang, Z., Wang, Y., Wang, D., Zheng, L., Wu, L., et al., 2022a. Simulation and prediction study of hydrogenation/dehydrogenation kinetics based on the universal changing-volume model. Chem. Eng. Sci. 251, 117428.
Jana, S., Muthukumar, P., 2021. Design and performance prediction of a compact MmNi4.6Al0.4 based hydrogen storage system. J. Energy Storage 39, 102612.
Luo, S., Clewley, J.D., Flanagan, T.B., Bowman, R.C., Wade, L.A., 1998. Further studies of the isotherms of LaNi5−xSnx–H for x=0–0.5. J. Alloy. Compd. 267 (1), 171–181.
Wjihi, S., Sellaoui, L., Bouzid, M., Dhaou, H., Knani, S., Jemni, A., et al., 2017. Theoretical study of hydrogen sorption on LaNi5 using statistical physics treatment: microscopic and macroscopic investigation. Int. J. Hydrog. Energy 42 (5), 2699–2712.
Shen, D., Zhao, C.Y., 2013. Thermal analysis of exothermic process in a magnesium hydride reactor with porous metals. Chem. Eng. Sci. 98, 273–281.
Yang, F.S., Meng, X.Y., Deng, J.Q., Wang, Y.Q., Zhang, Z.X., 2008. Identifying heat and mass transfer characteristics of metal hydride reactor during adsorption - Parameter analysis and numerical study. Int. J. Hydrog. Energy 33 (3), 1014–1022.
Mohammadshahi, S.S., Gould, T., Gray, E.M., Webb, C.J., 2016a. An improved model for metal-hydrogen storage tanks - Part 2: Model results. Int. J. Hydrog. Energy 41 (6), 3919–3927.
Jiao, K., Li, X.G., Yin, Y., Zhou, Y.B., Yu, S.H., Du, Q., 2012. Effects of various operating conditions on the hydrogen absorption processes in a metal hydride tank. Appl. Energy 94, 257–269.
Kumar, A., Raju, N.N., Muthukumar, P., 2021. Parametric studies on MmNi4.7Fe0.3 based reactor with embedded cooling tubes for hydrogen storage and cooling application. J. Energy Storage 35, 102317.
Mohan, G., Prakash Maiya, M., Srinivasa Murthy, S., 2007. Performance simulation of metal hydride hydrogen storage device with embedded filters and heat exchanger tubes. Int. J. Hydrog. Energy 32 (18), 4978–4987.
Bao, Z.W., Yang, F.S., Wu, Z., Cao, X.X., Zhang, Z.X., 2013. Simulation studies on heat and mass transfer in high-temperature magnesium hydride reactors. Appl. Energy 112, 1181–1189.
Patil, S.D., Ram Gopal, M., 2013. Analysis of a metal hydride reactor for hydrogen storage. Int. J. Hydrog. Energy 38 (2), 942–951.
Souahlia, A., Dhaou, H., Mellouli, S., Askri, F., Jemni, A., Ben Nasrallah, S., 2014. Experimental study of metal hydride-based hydrogen storage tank at constant supply pressure. Int. J. Hydrog. Energy 39 (14), 7365–7372.
Wang, C.S., Brinkerhoff, J., 2021. Predicting hydrogen adsorption and desorption rates in cylindrical metal hydride beds: Empirical correlations and machine learning. Int. J. Hydrog. Energy 46 (47), 24256–24270.
Li, D., Wang, Y., Wu, L., Yang, F., Wu, Z., Zheng, L., et al., 2020. Kinetics study on the nonlinear modified varying-size model of LaNi5 during hydrogenation/dehydrogenation. Chem. Eng. Sci. 214, 115439.
Lin, X., Zhu, Q., Leng, H.Y., Yang, H.G., Lyu, T., Li, Q., 2019. Numerical analysis of the effects of particle radius and porosity on hydrogen absorption performances in metal hydride tank. Appl. Energy 250, 1065–1072.
Hardy, B.J., Anton, D.L., 2009. Hierarchical methodology for modeling hydrogen storage systems. Part II: Detailed models. Int. J. Hydrog. Energy 34 (7), 2992–3004.
Muthukumar, P., Satheesh, A., Linder, M., Mertz, R., Groll, M., 2009. Studies on hydriding kinetics of some La-based metal hydride alloys. Int. J. Hydrog. Energy 34 (17), 7253–7262.
Nakagawa, T., Inomata, A., Aoki, H., Miura, T., 2000. Numerical analysis of heat and mass transfer characteristics in the metal hydride bed. Int. J. Hydrog. Energy 25 (4), 339–350.
Na Ranong, C., Lozano, G., Hapke, J., Roetzel, W., Fieg, G., Bellosta von Colbe, J., 2011. Application of Danckwerts-type boundary conditions to the modeling of the thermal behavior of metal hydride reactors. Chem. Eng. Sci. 66 (20), 4654–4662.
Song, J., Wang, Y., Li, S., He, C., Wang, D., Yang, F., et al., 2018. Numerical and experimental study of La–Ni hydriding kinetics based on the varying-size model. Chem. Eng. Sci. 176, 580–599.
Chung, C.A., Ho, C.J., 2009. Thermal-fluid behavior of the hydriding and dehydriding processes in a metal hydride hydrogen storage canister. Int. J. Hydrog. Energy 34 (10), 4351–4364.
Demircan, A., Demiralp, M., Kaplan, Y., Mat, M.D., Veziroglu, T.N., 2005. Experimental and theoretical analysis of hydrogen absorption in LaNi5-H-2 reactors. Int. J. Hydrog. Energy 30 (13-14), 1437–1446.
Nam, J., Ko, J., Ju, H., 2012. Three-dimensional modeling and simulation of hydrogen absorption in metal hydride hydrogen storage vessels. Appl. Energy 89 (1), 164–175.
Mohammadshahi, S.S., Gould, T., Gray, E.M., Webb, C.J., 2016b. An improved model for metal-hydrogen storage tanks - Part 1: Model development. Int. J. Hydrog. Energy 41 (5), 3537–3550.
Dhaou, H., Souahlia, A., Mellouli, S., Askri, F., Jemni, A., Ben Nasrallah, S., 2010. Experimental study of a metal hydride vessel based on a finned spiral heat exchanger. Int. J. Hydrog. Energy 35 (4), 1674–1680.
Garrison, S.L., Hardy, B.J., Gorbounov, M.B., Tamburello, D.A., Corgnale, C., vanHassel, B.A., et al., 2012. Optimization of internal heat exchangers for hydrogen storage tanks utilizing metal hydrides. Int. J. Hydrog. Energy 37 (3), 2850–2861.
Keshari, V., Maiya, M.P., 2018. Design and investigation of hydriding alloy based hydrogen storage reactor integrated with a pin fin tube heat exchanger. Int. J. Hydrog. Energy 43 (14), 7081–7095.
Manai, M.S., Leturia, M., Pohlmann, C., Oubraham, J., Mottelet, S., Levy, M., et al., 2019. Comparative study of different storage bed designs of a solid-state hydrogen tank. J. Energy Storage 26.
Raju, M., Kumar, S., 2012. Optimization of heat exchanger designs in metal hydride based hydrogen storage systems. Int. J. Hydrog. Energy 37 (3), 2767–2778.
Mellouli, S., Askri, F., Dhaou, H., Jemni, A., Ben Nasrallah, S., 2010. Numerical simulation of heat and mass transfer in metal hydride hydrogen storage tanks for fuel cell vehicles. Int. J. Hydrog. Energy 35 (4), 1693–1705.

Nyamsi, S.N., Yang, F.S., Zhang, Z.X., 2012. An optimization study on the finned tube heat exchanger used in hydride hydrogen storage system - analytical method and numerical simulation. Int. J. Hydrog. Energy 37 (21), 16078–16092.
Chandra, S., Sharma, P., Muthukumar, P., Tatiparti, S.S.V., 2020. Modeling and numerical simulation of a 5 kg LaNi5-based hydrogen storage reactor with internal conical fins. Int. J. Hydrog. Energy 45 (15), 8794–8809.
Ma, J.C., Wang, Y.Q., Shi, S.F., Yang, F.S., Bao, Z.W., Zhang, Z.X., 2014. Optimization of heat transfer device and analysis of heat & mass transfer on the finned multi-tubular metal hydride tank. Int. J. Hydrog. Energy 39 (25), 13583–13595.
Wang, J.S., Wang, X., 2016. The heat transfer optimization of conical fin by shape modification. Chin. J. Chem. Eng. 24 (8), 972–978.
Wang, H., Yi, G., Ye, J., Feng, X., Li, Z., Wang, S., et al., 2022b. Intensification of hydrogen absorption process in metal hydride devices with novel corrugated fins: A validated numerical study. J. Alloy. Compd. 926, 166759.
Bai, X.S., Yang, W.W., Tang, X.Y., Yang, F.S., Jiao, Y.H., Yang, Y., 2021. Optimization of tree-shaped fin structures towards enhanced absorption performance of metal hydride hydrogen storage device: A numerical study. Energy 220.
Krishna, K.V., Pandey, V., Maiya, M.P., 2022. Bio-inspired leaf-vein type fins for performance enhancement of metal hydride reactors. Int. J. Hydrog. Energy 47 (56), 23694–23709.
Singh, A., Maiya, M.P., Murthy, S.S., 2015. Effects of heat exchanger design on the performance of a solid state hydrogen storage device. Int. J. Hydrog. Energy 40 (31), 9733–9746.
Muthukumar, P., Madhavakrishna, U., Dewan, A., 2007. Parametric studies on a metal hydride based hydrogen storage device. Int. J. Hydrog. Energy 32 (18), 4988–4997.
Yang, F., Zhang, Z., 2011. Simulation Studies on the Coupling Process of Heat/Mass Transfer in a Metal Hydride Reactor. Mass Transf. Multiph. Syst. its Appl.
Anbarasu, S., Muthukumar, P., Mishra, S.C., 2014. Thermal modeling of LmNi(4.91)Sn (0.15) based solid state hydrogen storage device with embedded cooling tubes. Int. J. Hydrog. Energy 39 (28), 15549–15562.
Muthukumar, P., Singhal, A., Bansal, G.K., 2012. Thermal modeling and performance analysis of industrial-scale metal hydride based hydrogen storage container. Int. J. Hydrog. Energy 37 (19), 14351–14364.
Busque, R., Torres, R., Grau, J., Roda, V., Husar, A., 2017. Effect of metal hydride properties in hydrogen absorption through 2D-axisymmetric modeling and experimental testing in storage canisters. Int. J. Hydrog. Energy 42 (30), 19114–19125.
Busque, R., Torres, R., Grau, J., Roda, V., Husar, A., 2018. Mathematical modeling, numerical simulation and experimental comparison of the desorption process in a metal hydride hydrogen storage system. Int. J. Hydrog. Energy 43 (35), 16929–16940.
Lesmana, L.A., Aziz, M., 2023. Adoption of triply periodic minimal surface structure for effective metal hydride-based hydrogen storage. Energy 262, 125399.
Singh, A., Prakash Maiya, M., Srinivasa Murthy, S., 2017. Performance of a solid state hydrogen storage device with finned tube heat exchanger. Int. J. Hydrog. Energy 42 (43), 26855–26871.
Boukhari, A., Bessaïh, R., 2015. Numerical heat and mass transfer investigation of hydrogen absorption in an annulus-disc reactor. Int. J. Hydrog. Energy 40 (39), 13708–13717.
Cao, X., Yang, F.-S., Wu, Z., Wang, Y.Q., Zhang, Z.-x, 2013. Experimental Study on the Hydrogen Storage Properties of LaNi5 Alloy in Repeated Hydriding/Dehydriding Cycles. Adv. Mater. Res. 815, 25–30.